

# Constraints on interactions between aerosols and clouds on a global scale from a combination of MODIS-CERES satellite data and climate simulations

X. Ma<sup>1,2</sup>, K. von Salzen<sup>1,2</sup>, and J. Cole<sup>2</sup>

<sup>1</sup>University of Victoria, Victoria, British Columbia, Canada

<sup>2</sup>Canadian Centre for Climate Modelling and Analysis, Environment Canada, Victoria, British Columbia, Canada

Received: 11 May 2010 – Published in Atmos. Chem. Phys. Discuss.: 7 June 2010

Revised: 24 September 2010 – Accepted: 11 October 2010 – Published: 19 October 2010

**Abstract.** Satellite-based cloud top effective radius retrieved by the CERES Science Team were combined with simulated aerosol concentrations from CCCma CanAM4 to examine relationships between aerosol and cloud that underlie the first aerosol indirect (cloud albedo) effect. Evidence of a strong negative relationship between sulphate, and organic aerosols, with cloud top effective radius was found for low clouds, indicating both aerosol types are contributing to the first indirect effect on a global scale. Furthermore, effects of aerosol on the cloud droplet effective radius are more pronounced for larger cloud liquid water paths. While CanAM4 broadly reproduces the observed relationship between sulphate aerosols and cloud droplets, it does not reproduce the dependency of cloud top droplet size on organic aerosol concentrations nor the dependency on cloud liquid water path. Simulations with a modified version of the model yield a more realistic dependency of cloud droplets on organic carbon. The robustness of the methods used in the study are investigated by repeating the analysis using aerosol simulated by the GOCART model and cloud top effective radii derived from the MODIS Science Team.

from simple empirical relationships between cloud droplet and aerosol concentrations to more rigorous parameterizations for activation of aerosol particles to cloud droplets. Twomey (1974) first found that cloud reflectance increases with aerosol particle concentration for constant cloud water content since aerosols can act as cloud condensation nuclei (CCN). This is called the cloud albedo effect, i.e. first indirect effect.

To evaluate the ability of the ECHAM GCM to simulate the first aerosol indirect effect (Lohmann and Lesins, 2002), POLDER satellite retrievals were used to examine the relationship between cloud droplet effective radius and aerosol index (AI). It was found that cloud droplet radius decreased with increasing AI, according to satellite data and model output, and that the relationship was more pronounced in the ECHAM GCM. Again using data from POLDER, Quaas et al. (2004) characterized aerosol impacts on clouds by accounting for variations in cloud liquid water path (LWP). In a later study, Quaas et al. (2008) used data from the Cloud and the Earth's Radiant Energy System (CERES, Wielicki et al., 1996) and the MODerate Resolution Imaging Spectroradiometer (MODIS, Remer et al., 2005) to derive a statistical relationship between cloud properties and column aerosol concentration. This latter study found a much weaker magnitude of the indirect effect compared to other estimates.

An effect of organic carbon on cloud droplet number concentrations and therefore indirect effects is expected from basic Köhler theory. However, the global magnitude of this effect has not yet been determined from global observations. As pointed out by Stevens and Feingold (2009) and others, competition between aerosol particles with different chemical composition and size tends to 'buffer' the indirect effect, causing a nonlinear dependency of cloud droplets on aerosol

## 1 Introduction

The representations of aerosol indirect effects, i.e. aerosol-cloud interactions, remains a source of large uncertainties in GCM simulations of climate change (IPCC, 2007). Representation of aerosol effects on clouds in GCMs range



Correspondence to: K. von Salzen  
(knut.vonsalzen@ec.gc.ca)

concentrations in the atmosphere. In general, there is a multitude of microphysical and dynamical processes that tend to buffer the response of clouds to aerosol changes, including variable precipitation susceptibility of shallow clouds and interactions between mixing of moisture, convection, precipitation, and radiation (Stevens and Feingold, 2009).

While it is not straightforward to determine the magnitudes, or even the signs, of different mechanisms through which organic carbon influences clouds and indirect effects, a more pragmatic approach would be to investigate whether any relationships can be observed between organic carbon and cloud properties on scales that are relevant to global climate. For instance, an anti-correlation between global organic carbon concentrations and cloud droplet sizes would indicate a likely contribution of organic carbon to global mean indirect aerosol forcings of climate. Furthermore, estimates of global relationships between organic carbon and cloud droplet sizes can be expected to be very useful for validation of global climate models.

This study focuses on the effect of sulphate and organic carbon aerosols on low clouds, i.e., clouds with tops below 700 hPa. In the earlier studies described above, the indirect effect was determined using passive measurements that were generally representative of the entire vertical column. Aerosol and clouds may occur at different heights in the atmosphere which can obscure local interactions between them. To reduce this possibility, aerosol concentrations within the same height range as low clouds were used, reducing some of the ambiguities caused by using quantities vertically integrated over the depth of the atmosphere like the aerosol index.

In contrast to several other studies, model results for dry aerosols rather than satellite-based estimates of AI are used in this study for the diagnosis of relationships between cloud microphysical properties and amounts of aerosol. With this approach, diagnosed relationships between clouds and aerosols are not affected by processes that potentially limit the usefulness of purely satellite-based relationships. Satellite-based results for AI or aerosol optical depth do not provide unbiased estimates of dry aerosol amounts given a typical lack of information about hygroscopic particle growth or omission of 3-D radiative transfer effects in the vicinity of clouds (Marshak et al., 2008).

## 2 Analysis technique

Observations of aerosol composition are only available for a relatively small number of land-based sites around the globe. However, 3-D concentrations for different types of aerosols are available from a number of global models (e.g. AeroCom project; Textor et al., 2006). While different models can have substantial differences in simulated aerosol life cycles, basic features of simulated aerosol concentration fields are similar for most global aerosol models. For instance, simulated near-

surface sulphate concentrations usually vary by several orders of magnitude between polluted regions in the Northern Hemisphere and more remote regions in the Southern Hemisphere, similar to observations (e.g. Chin et al., 1996).

Arguably, large differences in hydrophilic (i.e. cloud-active) accumulation mode aerosol concentrations between different regions should be associated with detectable differences in cloud droplet sizes following the first aerosol indirect effect. For example, relationships between cloud droplet effective radius in low clouds and associated aerosol concentrations can be obtained from GCMs. They may also be obtained by combining long-term simulated aerosol concentrations and long-term satellite-based retrievals of cloud droplet effective radius. For sufficiently long averaging time periods, weather-related variations of accumulation mode aerosol and cloud properties can be expected to be small compared to climatological features.

For this study, global distributions of dry aerosol concentrations below 700 hPa were obtained from simulations with a developmental version of the CCCma 4th generation atmospheric general circulation model (CanAM4, von Salzen et al., 2005). These were subsequently used to diagnose relationships between aerosols and global satellite retrievals for the cloud droplet effective radius. In addition, cloud droplet effective radius simulated by CanAM4 were used to test whether the model is able to reproduce observed relationships between aerosols and cloud droplet effective radius.

The focus in the study is on low cloud properties retrieved by the CERES Science Team from MODIS observations, called MODIS-CE hereafter (Minnis et al., 2010, submitted). Only regions equatorward of 60° are used to reduce the possibility of retrievals in the presence of persistent and extensive regions of mixed and ice phase clouds. According to independent satellite retrievals for liquid and ice water path from the ISCCP-like CERES product [http://eosweb.larc.nasa.gov/PRODOCS/ceres/level3\\_iscsp-d2like\\_table.html](http://eosweb.larc.nasa.gov/PRODOCS/ceres/level3_iscsp-d2like_table.html), the mean fraction of monthly-mean liquid water clouds to total condensate (liquid + ice) for low clouds was very close to one for most of the region between 60° S and 60° N in July 2004.

The time period of MODIS-CE used here is from 2001 to 2005. Seasonal mean results for the time period June, July and August (JJA), and December, January and February (DJF) are used for the study. Since results for both seasons lead to similar conclusions, only results for JJA are shown here.

## 3 Model description

The spectral resolution of CanAM4 corresponds to a spherical harmonic expansion triangularly truncated at total wave number 63. There are 35 layers in the vertical with a monotonically increasing grid spacing with height, starting at a

grid spacing of approximately 100 m near the surface and up to the model top at approximately 1 hPa.

A climatological-mean annual cycle of sea surface temperature (SST) and sea ice boundary conditions were used in the simulations and were computed from fields used in the second phase of the Atmospheric Model Intercomparison Project (Taylor et al., 2000) by averaging over the period January 1956 through December 2000. These boundary conditions were used to perform CanAM4 simulations with a 5-month spinup period, which was discarded, and then to generate 5-year climatologies for analysis.

CanAM4 uses a bulk aerosol scheme, i.e. aerosol size distribution is not prognosed. The prognostic aerosol species in CanAM4 include sulphate, hydrophylic and hydrophobic organic carbon (OC), hydrophylic and hydrophobic black carbon (BC), sea salt, and mineral dust (Lohmann et al., 1999; Croft et al., 2005). Emissions in this study are from the AeroCom project for the year 2000 (Textor et al., 2006; Kinne et al., 2006), which provides the aerosol emission data from both natural and anthropogenic sources.

Transport, dry and wet deposition, and chemical reactions of the species are calculated in the GCM. The dry deposition flux is proportional to the aerosol concentration in the lowest model level and a dry deposition velocity (Lohmann et al., 1999). In-cloud scavenging by precipitation is calculated explicitly using the model-generated precipitation rate (Giorgi and Chameides, 1986), while below-cloud scavenging is parameterized according to Berge (1993) assuming a mean collection efficiency.

Similar to earlier work by Boucher and Lohmann (1995) and others, the cloud droplet number ( $N_c$ ) in CanAM4 is empirically related to the concentration of sulphate aerosol ( $SO_4$ ). Dufresne et al. (2005) adjusted the empirical constants in the parameterization for  $N_c$  by fitting GCM results to globally observed results for the cloud droplet effective radius from satellite. A slightly modified version of their parameterization is used in CanAM4, based on a comparison between model results and MODIS-CE retrievals for cloud droplet effective radius giving

$$N_c = 60(SO_4^{0.2}) \quad (1)$$

where  $N_c$  is in droplets  $cm^{-3}$  and  $SO_4$  in  $\mu g m^{-3}$  and a lower bound of 1 droplet  $cm^{-3}$  is used for  $N_c$ .

A fully prognostic single-moment cloud microphysics scheme is used in the model, based on the work of Lohmann and Roeckner (1996), Rotstain (1997) and Khairoutdinov and Kogan (2000). A statistical approach is used for microphysical properties of layer clouds (Chaboureaud and Bechtold, 2005). Radiative transfer is handled using a correlated-k distribution model (Li, 2002; Li and Barker, 2002, 2005) to describe the optical properties of gases and the Monte Carlo Independent Column Approximation (McICA) to treat radiative transfer in cloudy atmospheres (Pincus et al., 2003; Barker et al., 2008). The effect of aerosols on the formation of precipitation are not considered in the version of

the CanAM4 used for this study, i.e. no cloud lifetime effect. A constant cloud droplet number concentration of  $N_c = 50 cm^{-3}$  is used in the parameterization by Khairoutdinov and Kogan (2000).

There are several possibilities to compare cloud top effective radii simulated by GCMs with satellite-based retrievals. For this study, we use a modified version of the ISCCP simulator (Klein and Jacob, 1999) which emulates cloud-related variables that are comparable with data provided by MODIS-CE. These include cloud amount, cloud top pressure, cloud optical thickness, cloud water path and cloud top effective radius for clouds in four pressure ranges used by MODIS-CE. Input for the simulator are subcolumns created by a stochastic cloud generator (Räisänen et al., 2004), which are also provided to McICA for radiative transfer calculations.

The cloud top effective radius was approximated for each subcolumn by averaging from liquid cloud top, determined by the ISCCP simulator, downward to an optical depth of 3, by using  $\bar{r}_{eff} = \sum LWP_i / (\sum LWP_i / r_{eff,i})$ , where  $LWP_i$  and  $r_{eff,i}$  are the model layer liquid water path and effective radius. This was done instead of using the effective radius from the uppermost cloud layer (Quaas et al., 2004). The study of Platnick (2000) suggests that cloud effective radii retrieved at visible and near-infrared wavelengths contain information from the first few optical thicknesses below cloud top. In this version of CanAM4, it was found that the upper liquid cloud layer often had a cloud optical depth greater than 3 (not shown) and therefore the diagnosed cloud effective radius was often taken from the uppermost cloudy layer. However, by using the mean over a prescribed optical thickness our definition is independent of changes to model configuration, e.g., vertical resolution decreasing the layer optical thickness.

#### 4 Aerosol concentrations and cloud effective radius

Simulated sulphate ( $SO_4$ ) and hydrophilic organic carbon (OC) concentrations at low level (surface to 700 hPa) from CanAM4 are shown in Fig. 1. For sulphate, concentration maxima over North America, Europe, and Asia are mainly due to emissions from industrial fossil fuel burning. Secondary maxima are found downwind of major emission sources and South America because of biomass burning. Results for OC are dominated by biomass burning emissions from South America and South Africa.

Aerosol burdens and deposition fluxes from CanAM4 and other GCMs are listed in Table 1. Average results for ten climate models from the AeroCom project are also shown for comparison. Overall, CanAM4 simulated aerosol burdens and deposition rates agree well with mean results from the other GCMs. However, for both sulphate and particulate organic matter (POM), CanAM4 produces higher dry deposition and slightly lower wet deposition rates than the mean AeroCom model.

**Table 1.** Global annual averaged aerosol burden (unit: Tg), dry and wet deposition fluxes (unit: Tg/yr) from CanAM4 and various global models from the AeroCom project. AeroCom mean model results are also listed.

	Sulphate			POM		
	Burden	Dry depos.	Wet depos.	Burden	Dry Depos.	Wet Depos.
CanAM4	1.81	22.9	139.8	1.20	20.3	49.1
ARQM	3.47	25.6	105.9	4.06	94.8	77.3
DLR	2.62	6.5	184.9	1.33	7.1	59.2
GISS	1.46	19.2	78.1	1.22	19.3	45.5
KYU	0.95	20.6	117.2	1.61	N/A	N/A
LOA	2.91	0.0	209.9	1.35	0.0	65.5
MATCH	1.69	20.4	132.1	1.35	18.8	65.6
MOZGN	2.58	N/A	N/A	1.03	N/A	N/A
UIO-CTM	1.50	21.4	148.8	1.05	5.7	61.2
UIO-GCM	1.51	13.2	136.0	0.86	13.8	52.2
LSCE	2.61	17.1	159.1	1.59	15.8	49.6
AeroCom mean	2.10	20.4	142.0	1.30	13.0	53.0

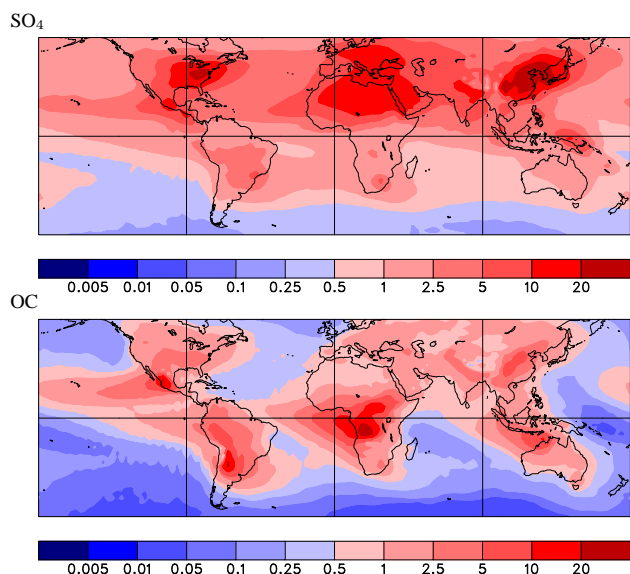


**Fig. 1.** Vertically-integrated sulphate ( $\text{SO}_4$ ) and hydrophylic organic carbon (OC) concentrations for low level (surface to 700 hPa) in JJA from CanAM4 simulations. Unit:  $\text{mg/m}^2$

The cloud top effective radius ( $r_{\text{eff}}$ ) from MODIS-CE for low clouds is shown in Fig. 2 (top panel). Large cloud droplets are mainly found over the ocean, where aerosol particle concentrations are low, while cloud droplets are smaller over land. Very large values over Africa are likely caused by less accurate retrieval over bright and dust-laden deserts, and are excluded from this study. The simulated cloud effective radius from CanAM4 in Fig. 2 (bottom panel) is characterized by large values over the ocean and smaller values over land. A qualitatively similar contrast between land and ocean

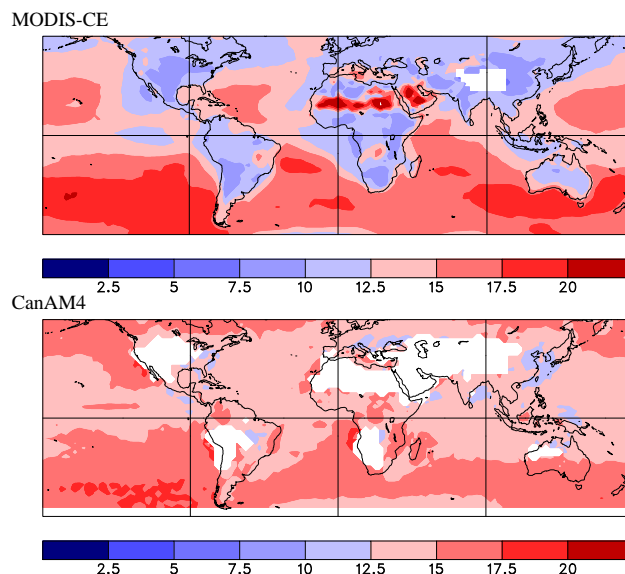


**Fig. 2.** Cloud top effective radius from MODIS-CE and CanAM4 for low level (surface to 700 hPa) in JJA. Unit:  $\mu\text{m}$

is also found for the MODIS-CE data. However, the modelled  $r_{\text{eff}}$  is generally smaller than the MODIS-CE retrievals over the Southern ocean, but larger than the MODIS-CE retrievals in the Northern Hemisphere. While differences are substantial for some regions, zonal mean results are in reasonable agreement at most latitudes (Fig. 7).

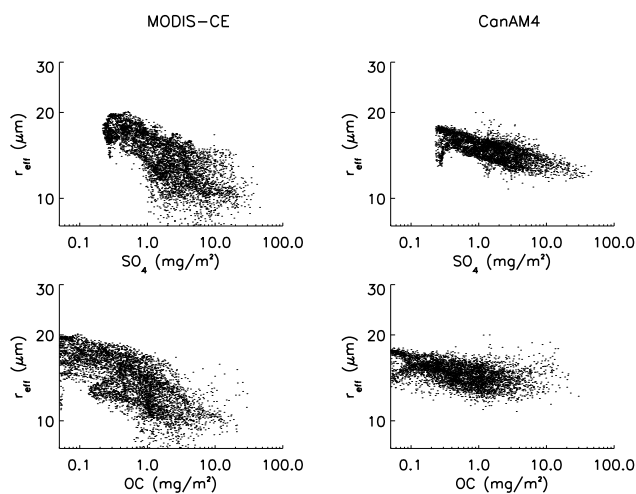


**Fig. 3.** Cloud effective radius ( $r_{\text{eff}}$ ) versus aerosol concentrations in JJA for low level (surface to 700 hPa). The concentrations of sulphate ( $\text{SO}_4$ ) and hydrophylic organic carbon (OC) are taken from the CanAM4 simulations while  $r_{\text{eff}}$  is from MODIS-CE retrievals (left column) and CanAM4 (right column).

## 5 Dependency of cloud droplet size on dry aerosol concentration

Figure 3 shows relationships between cloud top effective radius and dry aerosol concentrations in JJA for low clouds with tops below 700 hPa using data from all grid points in the MODIS-CE and model data sets between  $60^\circ$  S and  $60^\circ$  N. The same resolution ( $128 \times 64$  grid points) is used for both data sets. Data from high latitudes is excluded due to potential difficulties retrieving cloud microphysical properties over bright surface conditions, such as snow and sea ice, as well as more frequent mixed-phase cloud conditions.

According to Fig. 3,  $r_{\text{eff}}$  decreases with increasing concentrations of  $\text{SO}_4$  for both MODIS-CE and the GCM (upper panel). This behaviour is broadly consistent with relationships between cloud droplet size and aerosol index from previous studies (Lohmann and Lesins, 2002; Quaas et al., 2008). Cloud top droplet size from MODIS-CE also decreases with increasing concentrations of hydrophylic OC, indicating a potential contribution of OC to the first indirect effect. Interestingly, simulated results for  $r_{\text{eff}}$  also yield a slight decrease in size with OC although there is no contribution of OC to cloud droplet number according to Eq. 1. Apparently the relatively simple analysis above is not sufficient for detecting potential effects of OC on cloud droplets because correlations between OC and  $\text{SO}_4$  are not accounted for.

In order to determine relative contributions of  $\text{SO}_4$  and OC to the first indirect effect more accurately, results for  $r_{\text{eff}}$  were further stratified using cloud liquid water content (Fig. 4 and Fig. 5). According to Twomey (1974), increased concentrations of atmospheric aerosol will result in higher concentrations of cloud condensation nuclei (CCN), increased

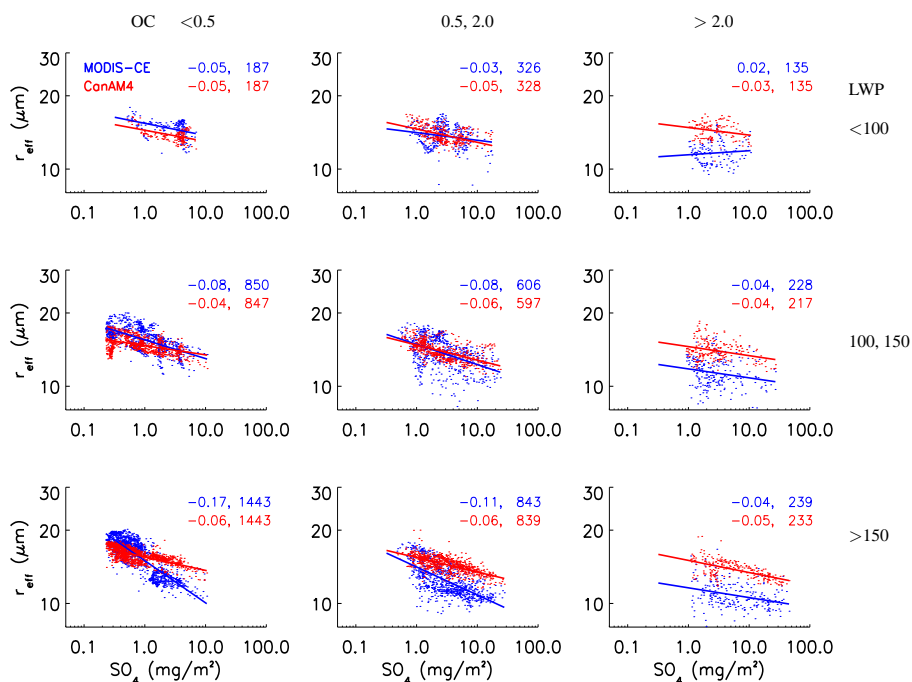
cloud droplet concentrations, and therefore smaller droplets. The hypothesis underlying the first indirect effect applies to clouds of equal liquid water content (LWC). Although important, this was largely omitted in previous studies of indirect effects using satellite-based data, mainly due to observational constraints.

Figure 4 shows relationships between  $r_{\text{eff}}$  and  $\text{SO}_4$ , for which the data for  $r_{\text{eff}}$  and  $\text{SO}_4$  were stratified according to three LWP categories, using simulated results for the LWP from the model. Furthermore, in order to distinguish the contributions from  $\text{SO}_4$  and OC, the data were also stratified according to three categories of OC in each LWP category. The linear regression results by least squares for each category are also shown. For all LWP and OC categories,  $r_{\text{eff}}$  decreases with increasing concentration of  $\text{SO}_4$  (except for the case with low LWP and large OC, there is a slight increase). The mean slope from CanAM4 for  $d \log(r_{\text{eff}})/d \log(\text{SO}_4)$  is close to  $-0.05$ , with a range from  $-0.03$  to  $-0.06$ , which is in reasonably good agreement with the theoretical value of  $-0.067$  according to Eq. 1. On the other hand, the diagnosed slope for the MODIS-CE results is in the range from  $-0.01$  to  $-0.17$ , indicating that the observed relationship between aerosol and cloud is fundamentally more complex than assumed in the model. Model results and observations agree well at intermediate values of the LWP and OC concentrations. The model tends to overestimate the dependency of the cloud droplet size on  $\text{SO}_4$  at low LWP and underestimate it at high LWP.

Figure 5 is similar to Fig. 4, except results are shown for OC instead of  $\text{SO}_4$ . Results for  $r_{\text{eff}}$  from CanAM4 do not show any significant increase or decrease with OC concentrations, with a diagnosed slope around zero, as theoretically expected from Eq. 1. However, the slope is negative for MODIS-CE results, with values ranging from 0 to  $-0.09$ . According to these results, effects of OC on cloud droplet size are potentially of the same order of magnitude as effects of  $\text{SO}_4$ , an effect that is apparently missing from CanAM4.

In order to summarize the findings described above, the data were stratified into more categories, i.e. ten categories for sulphate ranging from 0.1 to  $100.0 \text{ mg/m}^3$  and OC concentrations ranging from 0.01 to  $10.0 \text{ mg/m}^3$ . The dependency of  $r_{\text{eff}}$  on  $\text{SO}_4$  and OC is shown in Fig. 6. As shown before, simulated values of  $r_{\text{eff}}$  generally decrease with increasing sulphate concentration with no obviously systematic dependency on OC concentration. In contrast,  $r_{\text{eff}}$  from MODIS-CE clearly decreases with increasing aerosol concentrations. In particular, there is a dependency of  $r_{\text{eff}}$  on OC according to MODIS-CE results, giving evidence for a substantial contribution of OC to the first indirect effect. The omission of this effect in CanAM4 is evident for all LWP categories, indicating a shortcoming of the parameterized effect of aerosols on clouds.

As mentioned in Sect. 3, the model does not include a parameterization for cloud lifetime effects, which one may, in principle, expect to affect the cloud droplet radius.



**Fig. 4.** Low (surface to 700 hPa) cloud effective radius (in  $\mu\text{m}$ ) from MODIS-CE (in blue) and CanAM4 (in red) versus sulphate ( $\text{SO}_4$ ) concentrations in JJA. The data were stratified for 3 categories of liquid water path (LWP, in  $\text{g}/\text{m}^2$ ), and 3 categories of hydrophylic organic carbon (OC, in  $\text{mg}/\text{m}^2$ ). The slopes and numbers from linear regression are also marked in the plots.

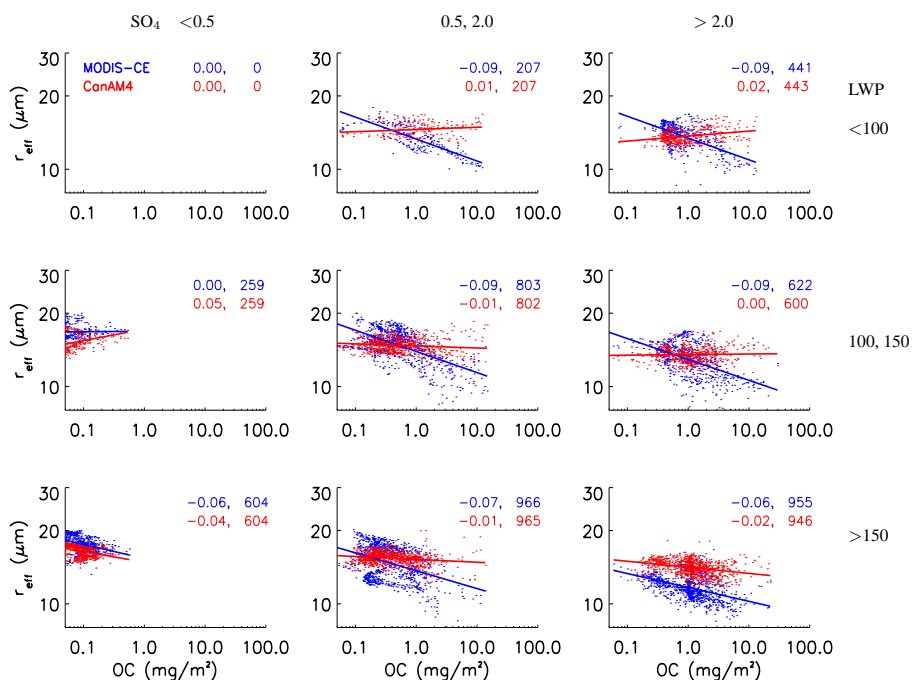


**Fig. 5.** Low (surface to 700 hPa) cloud effective radius (in  $\mu\text{m}$ ) from MODIS-CE (in blue) and CanAM4 simulation (in red) versus hydrophylic organic carbon (OC) in JJA. The data were stratified for 3 categories of liquid water path (LWP, in  $\text{g}/\text{m}^2$ ), and 3 categories of sulphate ( $\text{SO}_4$ , in  $\text{mg}/\text{m}^2$ ). The slopes and numbers from linear regression are also marked in the plots.

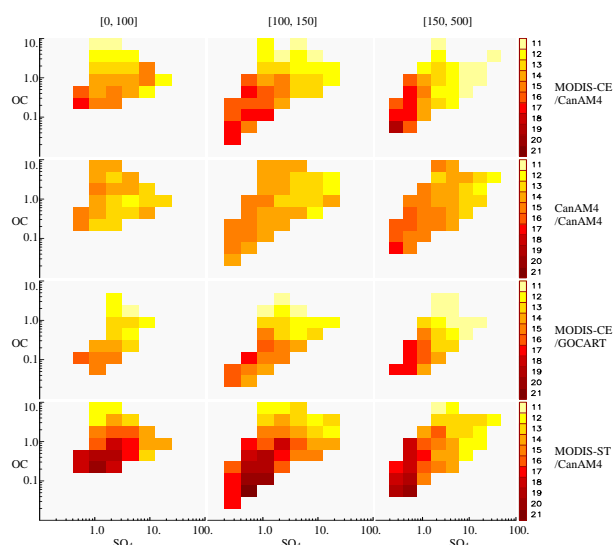


**Fig. 6.** Cloud effective radius (in  $\mu\text{m}$ ) as a function of sulphate and organic carbon concentrations (units:  $\text{mg}/\text{m}^2$ ). Results for effective radius from MODIS-CE (top panel), CanAM4 (second panel) using aerosol concentrations from CanAM4. Results for effective radius from MODIS-CE and simulated aerosol concentrations from GOCART, and the results for effective radius from MODIS-ST and simulated aerosol concentrations from CanAM4 are shown in the third and bottom panel, respectively. The data were stratified by using cloud liquid water path from CanAM4 simulations (columns, units:  $\text{g}/\text{m}^2$ ).

Consequently, one would not expect the model to successfully reproduce features of the satellite retrievals that are related to cloud lifetime effects. However, it seems possible that this effect is subtle for global mean relationships between aerosol and cloud droplet sizes. This may not be easy to detect based on the diagnostic approach in this study, which was designed to address very broad features of aerosol/cloud interactions. It seems likely that larger discrepancies between model results and satellite retrievals may be found if relationships are analyzed at smaller spatial and temporal scales than in this study. Generally, a realistic representation of relationships between aerosols and cloud droplet sizes appears to be a necessary, but not sufficient, criterion for an accurate representation of aerosol indirect effects in models.

## 6 Robustness of results

In order to test the robustness of our analysis, simulated aerosol concentrations from GOCART (Chin et al., 2001) for the period 2001–2005 were used instead of those from CanAM4. The GOCART model is a global model with a horizontal resolution of  $144 \times 91$  grid points and 31 vertical levels. It uses a bulk scheme to model sulphate as well as hydrophilic and hydrophobic BC and OC and a bin scheme is

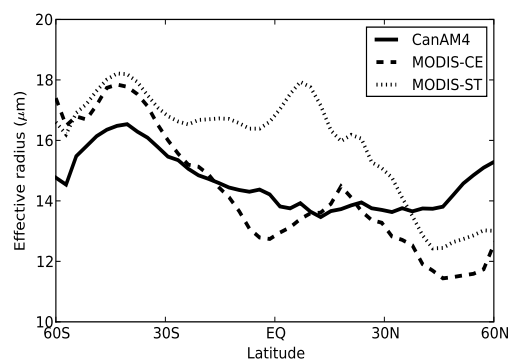


**Fig. 7.** Zonal mean cloud top effective radius in JJA from CCCma CanAM4, MODIS-CE and MODIS-ST.

used to model size distributions for sea salt and mineral dust. Assimilated meteorological fields from the NASA Goddard Earth Observing System Data Assimilation System (GEOS DAS) is provided to GOCART.

The relationship between values of  $r_{\text{eff}}$  from MODIS-CE and aerosol concentrations from GOCART are shown in Fig. 6 (third panel). Overall, there is good agreement with the results using aerosol concentrations from CanAM4 and MODIS-CE  $r_{\text{eff}}$ , i.e. a strong anti-correlation is also found between OC and  $r_{\text{eff}}$ .

In order to investigate uncertainties associated with satellite retrievals of cloud properties, climatological results retrieved from MODIS Science Team (MODIS-ST hereafter) for low clouds in JJA, averaged over 2001–2005, were also used. Like the MODIS-CE data, level 3 MODIS data from Terra was used (Hubanks et al., 2008). Figure 7 compares the climatological zonal mean cloud top effective radius from CanAM4, MODIS-CE and MODIS-ST for clouds with cloud top pressure greater than 700 hPa. The differences between the MODIS-CE and MODIS-ST retrieved values can in part be attributed to differing retrievals (Minnis et al., 2010) and provide a sense of the observational range relative to what is diagnosed from CanAM4. There is broad agreement between results from CanAM4, MODIS-CE and MODIS-ST. For all data sets, the cloud effective radius increases from north to south, although there is a clear difference poleward of  $30^\circ\text{N}$  with CanAM4 systematically simulating cloud top effective radii that are too large relative to MODIS-ST and MODIS-CE. CanAM4 also simulates a somewhat weaker change between the Northern and Southern Hemisphere.

The impact of uncertainties in satellite retrievals of cloud top effective radius on the analysis described above was tested by replacing  $r_{\text{eff}}$  MODIS-CE with those from MODIS-ST (bottom row, Fig. 6). Mean values of liquid low cloud  $r_{\text{eff}}$  for MODIS-ST were computed from joint histogram of liquid cloud top pressure and effective radius. Although there are some large regional differences between  $r_{\text{eff}}$  from MODIS-ST and MODIS-CE, the dependency of  $r_{\text{eff}}$  on aerosol concentrations is similar for both data sets.

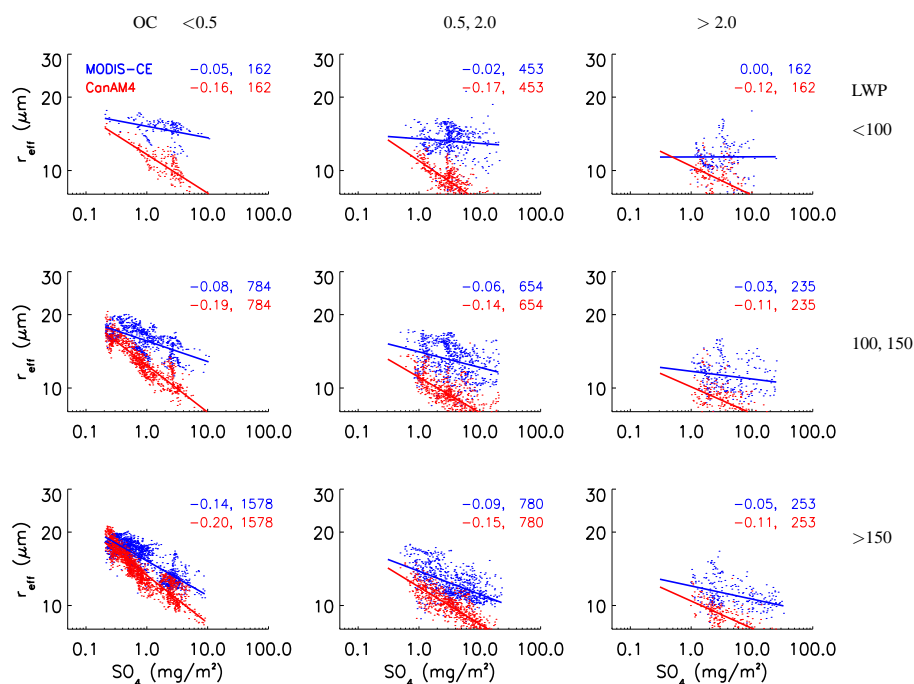


**Fig. 8.** Same as Fig. 4, but the simulation uses Menon's parameterization for CDNC.

Additional uncertainties in the analysis may arise from the omission of subgrid-scale distributions of clouds and aerosols. The objective for this study was to obtain broad relationships between aerosol and clouds using mean, all-sky aerosol amounts from the GCM. Given the limited resolution of the GCM and satellite data sets, it does not appear to be practical, nor appropriate, to use below-cloud aerosol concentrations, as is common practice in more detailed studies on interactions of aerosols and clouds that are based on observations from aircraft. This may bias the results because concentrations below cloud may be systematically different from all-sky concentrations. However, the magnitude and sign of a potential bias is unknown owing to various non-linear interactions between aerosols and clouds (Stevens and Feingold, 2009).

While potential biases from omission of subgrid-scale distributions of clouds and aerosols cannot be ruled out, this does not necessarily limit the usefulness of relationships between cloud droplet size and aerosol amounts from satellite and GCMs. In each case, the relationships are based on mean results for clouds and aerosols, so one may expect the relationships all to be affected by similar biases.

## 7 Model modifications

Results in the previous section provide evidence for the need to include effects of OC on cloud droplets in climate models. A bulk parameterization for cloud droplet number concentration, which includes effects of OC and sea salt aerosol, was

proposed by Menon et al. (2001). The relationships below were used to perform an additional simulation with CanAM4 for predictions of cloud droplet number for land,  $N_{\text{land}}$  and ocean,  $N_{\text{ocean}}$ .

$$N_{\text{land}} = 10^{2.41+0.50\log(\text{SO}_4)+0.13\log(\text{OM})} \quad (2)$$

$$N_{\text{ocean}} = 10^{2.41+0.50\log(\text{SO}_4)+0.13\log(\text{OM})+0.05\log(\text{Seasalt})} \quad (3)$$

where OM refers to the concentration of organic matter ( $\text{OM}=1.4\text{OC}$ ).

The resulting relationships this simulation are shown in Figs. 8 and 9. In contrast to the results from the original parameterization, Eq. (1),  $r_{\text{eff}}$  decreases too strongly with increasing  $\text{SO}_4$ . However, there is now good agreement between model results and observations for the dependency of  $r_{\text{eff}}$  on OC. The first indirect effect from  $\text{SO}_4$  is higher with the parameterization in Eqs. (2) and (3) than in the original simulation. Overall, contributions of OC to the first indirect effect are apparently well reproduced by this parameterization. However, it should be noted that  $N_{\text{land}}$  and  $N_{\text{ocean}}$  in Eqs. (2) and (3) tend to become independent of the sulphate concentration as OC tends to zero. It is unclear how this somewhat counterintuitive behaviour may have affected the results in Figs. 8 and 9.

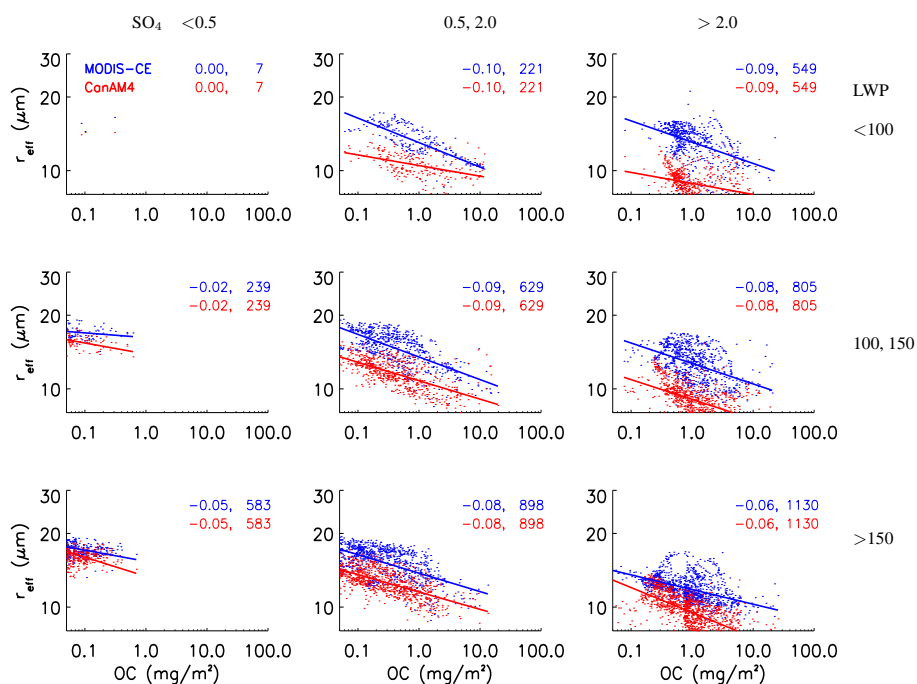


**Fig. 9.** Same as Fig. 5, but the simulation uses Menon's parameterization for CDNC.

## 8 Conclusions

Robust decreases in cloud top droplet effect radius with increasing concentrations of simulated sulphate and OC aerosol were found for low clouds based on a combination of satellite data and output from CanAM4. This is consistent with the hypothesis underlying the first indirect effect. Results presented in this study suggest that OC may have similar efficiency in affecting cloud droplet sizes as sulphate on a global scale, indicating a potentially large contribution of OC to the first indirect effect.

CanAM4 produces relationships between cloud droplet size and sulphate concentrations that are similar, giving evidence for an overall realistic representation of the first indirect effect due to sulphate aerosol on a global scale. However, the model does not reproduce a decrease in cloud droplet sizes with increasing OC concentrations, a relationship that was found when using satellite-based retrievals of cloud droplet sizes. The relationships between cloud droplet sizes and aerosol amounts indicate a weaker increase of the indirect effect with increasing LWP for CanAM4 than that diagnosed for MODIS-CE. A version of CanAM4 which accounts for a contribution of OC to cloud droplet number concentration (Menon et al., 2001) produced good agreement with MODIS-CE retrievals about the dependency of the droplet size on OC concentrations.

The causes for the increase in the magnitude of the first indirect effect with increasing cloud water path are not clear. However, it is possible that cloud dynamics can lead to dif-

ferences in the magnitude of the first aerosol indirect effect (Feingold, 2003). For example, larger updraft velocities in convective clouds likely lead to a stronger first indirect effect compared to lower updraft velocities in stably stratified stratiform clouds. The parameterization of cloud droplet number concentration currently used in CanAM4 does not account for differences in cloud dynamics.

It should be noted that while globally representative relationships between aerosol amounts and cloud droplet sizes will likely be very useful for studies of global climate, it is unlikely that similar relationships exist at regional and smaller scales. No direct information is available from the relationships about contributions from different mechanisms that contribute to overall aerosol indirect effects, some of which are highly variable in space and time. However, Avey et al. (2007) and Brioude et al. (2009) successfully demonstrated that a combination of data from satellite and tracer transport simulations can be used to determine aerosol effects on clouds on regional scales. By using a range of observational data and model output, there seem to be promising opportunities for research on aerosol indirect effects.

Relationships between cloud droplet effective radius and dry aerosol concentrations will be used in future comparisons of GCM simulations using more detailed representation of aerosol and cloud microphysical processes. For example, a future version of CanAM4 will include a parameterization for the activation of aerosol that accounts for contributions from sulphate, OC and other aerosol types.

*Acknowledgements.* We thank two anonymous reviewers and two internal reviewers (John Fyfe and Kirsten Zickfeld) for their very helpful comments and suggestions. We further thank Mian Chin for providing GOCART model results. MODIS-CERES data were obtained from the NASA Langley Research Center EOSDIS Distributed Active Archive Center and MODIS Science Team data were retrieved from the NASA Level 1 and Atmosphere Archive and Distribution System (LAADS). Funding for this study has been provided by the Canadian Foundation for Climate and Atmospheric Sciences (CFCAS) via the Cloud/Aerosol Feedbacks and Climate research network (CAFC) and Environment Canada.

Edited by: J. Quaas

## References

- Avey, L., Garrett, T. J., and Stohl, A.: Evaluation of the aerosol indirect effect using satellite, tracer transport model, and aircraft data from the International Consortium for Atmospheric Research on Transport and Transformation, *J. Geophys. Res.*, 112, D10S33, doi:10.1029/2006JD007581, 2007.
- Barker, H. W., Cole, J. N. S., Morcrette, J. J., Pincus, R., Raisanen, P., von Salzen, K., and Vaillancourt, P. A.: The Monte Carlo Independent Column Approximation: An assessment using several global atmospheric models, *Q. J. Roy. Meteorol. Soc.*, 134, 1463–1478, 2008.
- Berge, E.: Coupling of wet scavenging of sulphur to clouds in a numerical weather prediction model, *Tellus*, 45B, 1–22, 1993.
- Boucher, O. and Lohmann, U.: The sulfate-CCN-cloud albedo effect: a sensitivity study with two general circulation models, *Tellus*, 47B, 281–300, 1995.
- Brioude, J., Cooper, O. R., Feingold, G., Trainer, M., Freitas, S. R., Kowal, D., Ayers, J., Prins, E., Minnis, P., McKeen, S. A., Frost, G. J., and Hsie, E.-Y.: Effect of biomass burning on marine stratocumulus clouds off the California coast, *Atmos. Chem. Phys.*, 9, 8841–8856, doi:10.5194/acp-9-8841-2009, 2009.
- Chaboureaud, J.-P. and Bechtold, P.: Statistical representation of clouds in a regional model and the impact on the diurnal cycle of convection during tropical convection, cirrus and nitrogen oxides (TROCCINOX), *J. Geophys. Res.*, 110, D17103, doi:10.1029/2004JD005645, 2005.
- Chin, M., Jacob, D. J., Gardner, G. M., Spiro, P. A., Foreman-Fowler, M., and Savoie, D. L.: A global three-dimensional model of tropospheric sulfate, *J. Geophys. Res.*, 101, 18667–18690, 1996.
- Chin, M., Ginoux, P., Kinne, S., Torres, O., Holben, B. N., Duncan, B. N., Martin, R. V., Logan, J. A., and Higurashi, A.: Tropospheric aerosol optical thickness from GOCART model and comparisons with satellite and sun photometer measurements, *J. Atmos. Sci.*, 59, 461–483, 2001.
- Croft, B., Lohmann, U., and von Salzen, K.: Black carbon aging in the Canadian Centre for Climate modelling and analysis general circulation model, *Atmos. Chem. Phys.*, 5, 1383–1419, doi:10.5194/acp-5-1383-2005, 2005.
- Dufresne, J.-L., Quaas, J., Boucher, O., Denvil, S., and Fairhead, L.: Contrasts in the effects on climate of anthropogenic sulphate aerosols between the 20th and 21st century, *Geophys. Res. Lett.*, 32, L21703, doi:10.1029/2005GL023619, 2005.
- Feingold, G.: Modeling of the first indirect effect: Analysis of measurement requirements, *Geophys. Res. Lett.*, 230, doi:10.1029/2003GL017967, 2003.
- Giorgi, F. and Chameides, W. L.: Rainout lifetimes of highly soluble aerosols and gases inferred from simulations with a general circulation model, *J. Geophys. Res.*, 91, 14367–14376, 1986.
- Hubanks, P., King, M., Platnick, S., and Pincus, R.: MODIS Atmosphere L3 Gridded Product Algorithm Theoretical Basis Document, ATBD, Reference Number: ATBD-MOD-30, 2008.
- IPCC: Contribution of Working Group I to the Fourth Assessment report of the intergovernmental panel on climate change, Cambridge University Press, 2007.
- Khairoutdinov, M. and Kogan, Y.: A new cloud physics parameterization in a large-scale simulation model of marine stratocumulus, *Mon. Weather Rev.*, 128, 229–243, 2000.
- Kinne, S., Schulz, M., Textor, C., Guibert, S., Balkanski, Y., Bauer, S., Bernsten, T., Berglen, T., Boucher, O., Chin, M., Dentener, F., Diehl, T., Easter, R., Feichter, H., Fillmore, D., Ghan, S., Ginoux, P., Gong, S., Grini, A., Hendricks, J., Horowitz, L., Huang, P., Isaksen, I., Iversen, T., Kloster, S., Koch, D., Kirkevåg, A., Kristjansson, J., Krol, M., Lauer, A., Lamarque, J., Liu, X., Montanaro, V., Myhre, G., Penner, J., Pitari, G., Reddy, S., Seland, O., Stier, P., Takemura, T., and Tie, X.: An AeroCom initial assessment optical properties in aerosol component modules of global models, *Atmos. Chem. Phys.*, 6, 1815–1834, doi:10.5194/acp-6-1815-2006, 2006.
- Klein, S. A. and Jacob, C.: Validation and sensitivities of frontal clouds simulated by the ECMWF model, *Mon. Weather Rev.*, 127(10), 2514–2531, 1999.
- Li, J.: Accounting for unresolved clouds in a 1D infrared radiative transfer model. Part I: Solution for radiative transfer, including cloud scattering and overlap, *J. Atmos. Sci.*, 59, 3302–3320, 2002.
- Li, J. and Barker, H. W.: Accounting for unresolved clouds in a 1D infrared radiative transfer model. Part II: Horizontal variability of cloud water path, *J. Atmos. Sci.*, 59, 3321–3339, 2002.
- Li, J. and Barker, H. W.: A radiation algorithm with correlated-k distribution. Part I: local thermal equilibrium, *J. Atmos. Sci.*, 62, 286–309, 2005.
- Lohmann, U. and Lesins, G.: Stronger constraints on the anthropogenic indirect aerosol effect, *Science*, 298, 1012–1015, 2002.
- Lohmann, U. and Roeckner, E.: Design and performance of a new cloud microphysics scheme developed for the ECHAM general circulation model, *Clim. Dynam.*, 12, 557–572, 1996.
- Lohmann, U., von Salzen, K., McFarlane, N., Leighton, H. G., and Feichter, J.: Tropospheric sulphur cycle in the Canadian General Circulation Model, *J. Geophys. Res.*, 104, 26,833–26,858, 1999.
- Marshak, A., Wen, G., Coakley, J., Remer, L., Loeb, N. G., and Cahalan, R. F.: A simple model for the cloud adjacency effect and the apparent bluing of aerosols near clouds, *J. Geophys. Res.*, 113, D14S17, doi:10.1029/2007JD009196, 2008.
- Menon, S., Genio, A. D., Koch, D., and Tselioudis, G.: GCM Simulations of the Aerosol Indirect Effect: Sensitivity to Cloud Parameterization and Aerosol Burden, *J. Atmos. Sci.*, 59, 692–713, 2001.
- Minnis, P., Sun-Mack, S., Chen, Y., Khaiyer, M. M., Yi, Y., K. Ayers, J., Brown, R. R., Dong, X., Gibson, S. C., Heck, P. W., Lin, B., Nordeen, M. L., Nguyen, L., Palikonda, R., Smith, W. L., Spangenberg, D. A., Trepte, Q. Z., and Xi, B.: CERES Edition-2

- Cloud Property Retrievals Using TRMM VIRS and TERRA and AQUA MODIS Data, Part II: Examples of Average Results and Comparisons with Other data, Submitted to IEEE Trans. Geosci. Remote Sens., February, 2010.
- Pincus, R., Barker, H. W., and Morcrette, J. J.: A fast, flexible, approximate technique for computing radiative transfer in inhomogeneous cloud fields, *J. Geophys. Res.*, 110(D13), 4376, doi:10.1029/202JD003322, 2003.
- Platnick, S.: Vertical photon transport in cloud remote sensing problems, *J. Geophys. Res.*, 105, 22919–22935, 2000.
- Quaas, J., Boucher, O., and Breon, F. M.: Aerosol indirect effects in POLDER satellite data and the Laboratoire de Meteorologie Dynamique-Zoom (LMDZ) general circulation model, *J. Geophys. Res.*, 109, D08205, doi:10.1029/2003JD004317, 2004.
- Quaas, J., Bofeinuher, O., Bellouin, N., and Kinne, S.: Satellite-based estimate of the direct and indirect aerosol climate forcing, *J. Geophys. Res.*, 113, D05204, doi:10.1029/2007JD008962, 2008.
- Räsänen, P., Barker, H. W., Khairoutdinov, M. F., Li, J., and Randall, D. A.: Stochastic generation of subgrid-scale cloudy columns for large-scale models, *Q. J. Roy. Meteorol. Soc.*, 130, 2047–2067, doi:10.1256/qj.03.99, 2004.
- Remer, L., Kaufman, Y., Tanre, D., Mattoo, S., Chu, D., Martin, J., Li, R.-R., Ichoku, C., Levy, R., Kleidman, R., Eck, T., Vermote, E., and Holben, B.: The MODIS aerosol algorithm, products and validation, *J. Atmos. Sci.*, 62(4), 947–973, 2005.
- Rotstajn, L.: A physically based scheme for the treatment of stratiform clouds and precipitation in large-scale models. I: Description and evaluation of the microphysical processes., *Q. J. Roy. Meteorol. Soc.*, 123, 1227–1282, 1997.
- Stevens, B. and Feingold, G.: Untangling aerosol effects on clouds and precipitation in a buffered system, *Nature*, 461, 607–613, 2009.
- Taylor, K. E., Williamson, D., and Zwiers, F.: AMIP II sea surface temperature and sea ice concentration boundary conditions, 23 June 1997 (revised 6 April 2001), <http://www-pcmdi.llnl.gov/projects/amip/AMIP2EXPDSN/BCS/bcsintro.php>, 2000.
- Textor, C., Schulz, M., Guibert, S., Kinne, S., Balkanski, Y., Bauer, S., Bernsten, T., Berglen, T., Boucher, O., Chin, M., Dentener, F., Diehl, T., Easter, R., Feichter, H., Fillmore, D., Ghan, S., Ginoux, P., Gong, S., Grini, A., Hendricks, J., Horowitz, L., Huang, P., Isaksen, I., Iversen, T., Kloster, S., Koch, D., Kirkevg, A., Kristjansson, J., Krol, M., Lauer, A., Lamarque, J., Liu, X., Montanaro, V., Myhre, G., Penner, J., Pitari, G., Reddy, S., Seland, O., Stier, P., Takemura, T., and Tie, X.: Analysis and quantification of the diversities of aerosol life cycles within AeroCom, *Atmos. Chem. Phys.*, 6, 1777–1813, doi:10.5194/acp-6-1777-2006, 2006.
- Twomey, S.: Pollution and the planetary albedo, *Atmos. Environ.*, 8, 1251–1256, 1974.
- von Salzen, K., McFarlane, N. A., and Lazare, M.: The role of shallow convection in the water and energy cycles of the atmosphere, *Clim. Dynam.*, 25, 671–699, doi:10.1007/s00382-005-0051-2, 2005.
- Wielicki, B., Barkstrom, B., Harrison, E., Lee, R., Smith, G., and Cooper, J.: Clouds and the Earth's Radiant Energy System (CERES): An Earth Observing System experiment, *Bull. Am. Meteorol. Soc.*, 77, 853–868, 1996.